JACS
JOURNAL OF THE AMERICAN CHEMICAL SOCIETY
Article
pubs.acs.org/JACS

Identification of Surface Reactivity Descriptor for Transition Metal Oxides in Oxygen Evolution Reaction

Hua Bing Tao,[†] Liwen Fang,[‡] Jiazang Chen,[†] Hong Bin Yang,[†] Jiajian Gao,[†] Jianwei Miao,[†] Shengli Chen,[*,‡] and Bin Liu[*,†]

[†]School of Chemical and Biomedical Engineering, Nanyang Technological University, 62 Nanyang Drive, Singapore 637459, Singapore

[‡]College of Chemistry and Molecular Sciences, Wuhan University, Wuhan 430072, PR China

Supporting Information

ABSTRACT: A number of important reactions such as the oxygen evolution reaction (OER) are catalyzed by transition metal oxides (TMOs), the surface reactivity of which is rather elusive. Therefore, rationally tailoring adsorption energy of intermediates on TMOs to achieve desirable catalytic performance still remains a great challenge. Here we show the identification of a general and tunable surface structure, coordinatively unsaturated metal cation (M_{CUS}), as a good surface reactivity descriptor for TMOs in OER. Surface reactivity of a given TMO increases monotonically with the density of M_{CUS}, and thus the increase in M_{CUS} improves the catalytic activity for weak-binding TMOs but impairs that for strong-binding ones. The electronic origin of the surface reactivity can be well explained by a new model proposed in this work, wherein the energy of the highest-occupied d-states relative to the Fermi level determines the intermediates' bonding strength by affecting the filling of the antibonding states. Our model for the first time well describes the reactivity trends among TMOs, and would initiate viable design principles for, but not limited to, OER catalysts.

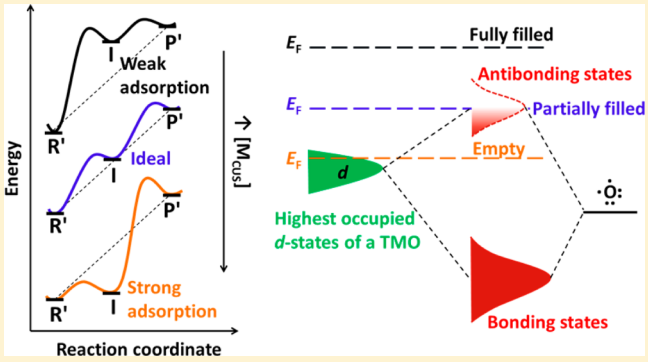

1. INTRODUCTION

Many electrochemical processes involve OER as the anodic reaction, some desire efficient OER catalysis (e.g., water electrolysis),[1,2] while the others need to suppress this reaction (e.g., Chlor-Alkali process).[3] Owing to the mismatch in adsorption energy of the multi-intermediates involved in the reaction,[4] OER is highly irreversible and thus usually manifests high overpotential (visualized in Figure S1). Because of the high working potential, OER takes place at oxidized surfaces and typical good OER catalysts are transition metal oxides (TMOs) and oxyhydroxides. Unraveling the behavior of OER catalysis on TMOs is of critical importance for both practical application and fundamental understanding of the interfacial chemistry.

Although intermediates' adsorption energy (corresponding to surface reactivity) describes the activity trend of OER on well-studied TMOs well,[5,6] the factors that govern the adsorption property or surface reactivity of TMOs still remain elusive. Besides, the critical working condition of OER makes it extremely difficult to directly measure the intermediates' adsorption property.[7] Therefore, effectively tailoring the adsorption energy of intermediates to achieve desirable OER activity is highly challenging. This frustrating outcome is in stark contrast to oxygen reduction reaction (ORR), the reverse reaction of OER, despite the same intermediates (OH*, O*, and OOH*) being involved in these two reactions. Unlike OER, ORR can be efficiently catalyzed by transition metals (TMs), whose surface reactivity can be well described by the d-band model,[8,9] which leads to successful catalyst design.[10,11] On the contrary, no general model exists to describe the surface reactivity of TMOs.[12,13]

The deduction of surface reactivity descriptor for TMOs is primarily prohibited by the extreme divergence in structure and properties of these materials,[14] in contrast to the relatively continuous variation in electronic structure and property of TMs. Nonetheless, several attempts have been made to correlate adsorption property with several features in the electronic structure of the oxides, including e_g filling for perovskites (AMO_3)[15,16] and the states' near-Fermi level for TiO_2[17] and 4d and 5d late TMOs.[18] Although the correlations describe the trends for the investigated materials well, no descriptor proves predictability in the well-studied group of OER catalysts such as Co_3O_4 and MnO_2. However, if we could avoid the complexity of TMOs and tune the surface electronic structure continuously, it could be possible to identify the surface reactivity descriptor for TMOs.

Received: May 25, 2016
Published: July 21, 2016

DOI: 10.1021/jacs.6b05398
J. Am. Chem. Soc. 2016, 138, 9978−9985

Here, we demonstrate that surface reactivity of a TMO for OER can be described well by a general, tunable surface structure, coordinatively unsaturated metal cation (M_{CUS}). Surface reactivity increases monotonically with the density of M_{CUS} (denoted as $[M_{CUS}]$); hence, weak-binding TMOs benefit from higher $[M_{CUS}]$ while strong-binding TMOs favor lower $[M_{CUS}]$ to achieve good OER catalytic activity. In our study, $[M_{CUS}]$ was carefully tuned by slight oxidation or reduction to prevent bulk structure or phase transition, which results in continuous variation in the surface electronic structure. We then propose that the energy of the highest occupied d-states of a TMO relative to its Fermi level describes the intermediate−surface bonding strength, which can be established as a universal descriptor for surface reactivity of TMOs.

2. RESULTS AND DISCUSSION

2.1. Surface Reactivity and Catalytic Performance of TiO_2 with Varying $[Ti_{CUS}]$. We first performed density functional theory (DFT) calculations to explore the correlation between adsorption energy with $[M_{CUS}]$ on rutile TiO_2 (110), a prototype model TMO for application in energy conversion. Rutile TiO_2 usually behaves as an n-type semiconductor and its extremely low surface reactivity could be improved by surface oxygen vacancy (O_V, corresponding to higher $[Ti_{CUS}]$ relative to the stoichiometric surface).[19,20] Herein, we systematically examined the influence of varying $[Ti_{CUS}]$ on the overall surface reactivity and OER activity. Owing to its inert surface, perfect rutile TiO_2 (110) adsorbs oxygen intermediates very weakly and features high OER overpotential, whereas creating more Ti_{CUS} monotonically enhances the intermediates adsorption and thus effectively changes the OER activity (Figure 1 and Figure S2). This trend is consistent with previous theoretical and experimental studies in which oxygen deficient surface showed higher reactivity with adsorbates (e.g., O_2 and H_2O)[19,21] and the enhanced reactivity is not constraint to O_V sites but delocalized.[22,23] The strong dependence of adsorption energy on $[Ti_{CUS}]$ indicates that Ti_{CUS} can be used as a descriptor for adsorption energy of OER intermediates on TiO_2.

To examine our theoretical prediction, we studied single-crystalline rutile TiO_2 nanorods with exposed (110) facets—the same ones used in our simulation. To increase $[Ti_{CUS}]$, the TiO_2 nanorods were slightly reduced to partially remove surface bridging oxygen. As shown in Figure S3, the bulk composition and structure of TiO_2 nanorods are well preserved after creation of additional Ti_{CUS}, whereas the surface structure and reactivity have been obviously modified (Figure 2). By ruling out bulk influence we could safely conclude that any difference in surface reactivity and catalytic performance should originate from Ti_{CUS}.

Both X-ray photoelectron spectroscopy (XPS) and O_2 temperature programed desorption (TPD) suggest the surface reactivity increases with $[Ti_{CUS}]$ (Figure 2a,b,c), well in line with our DFT calculation results. The O 1s spectrum (Figure 2a,b) suggests that dissociative O_2 adsorption (O_{ads}) on TiO_2 H-700 is significantly enhanced compared to pristine TiO_2. O_{ads} brings two effects: (i) the dissociative adsorption of water (OH_{ads}) is enhanced through the interaction between adsorbed water and O_{ads}[24,25] and (ii) electron transfer from Ti_{CUS} to O_{ads} makes the Ti 2p spectrum of TiO_2 H-700 invariant from that of TiO_2. That is why we observe enhanced OH_{ads} intensity in the O 1s spectrum but overlapped Ti 2p spectrum for TiO_2 H-700

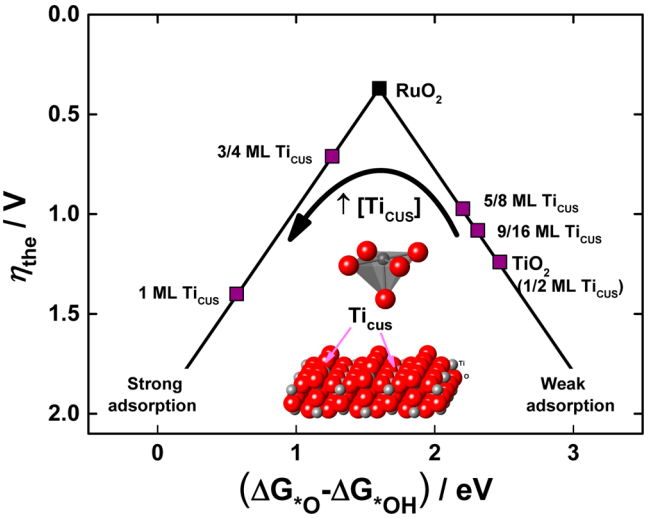

Figure 1. Dependence of theoretical overpotential (η_{the}) of rutile TiO_2 (110) in OER catalysis on $[Ti_{CUS}]$. η_{the} for RuO_2 is shown for comparison.[5] Inset shows the molecular structure of the rutile TiO_2 (110) surface, which is characterized by alternate rows of fivefold coordinated Ti (Ti_{5c}) and bridging O atoms (O_b). Underneath the O_b rows are the sixfold coordinated Ti (Ti_{6c}) rows. Ti_{6c} is fully coordinated by oxygen in a typical octahedral site, whereas the Ti_{5c} row and the O_V created Ti_{CUS} (denoted as O_v-Ti_{CUS}) in the Ti_{6c} row are coordinatively unsaturated and thus denoted as Ti_{CUS}. Different from Ti_{CUS} on the stoichiometric surface, O_v-Ti_{CUS} and Ti_{CUS} neighboring O_v are more reactive due to excess d-electrons.[22,23,42] The density of Ti_{CUS} is defined as the ratio of Ti_{CUS} to the sum of Ti_{5c} and Ti_{6c} rows. According to this definition, the perfect TiO_2 surface contains 1/2 ML (monolayer) Ti_{CUS}.

as compared to pristine TiO_2. O_2-TPD directly reveals the correlation between surface reactivity and $[Ti_{CUS}]$. The higher amount of desorbed O_2 from surfaces with higher $[Ti_{CUS}]$ indicates stronger adsorption. Moreover, the slightly reduced TiO_2 surface, e.g., TiO_2 H-700, could only be reoxidized at temperatures as high as 500 °C (Figure 2d). Such good stability can be attributed to the delocalization of unpaired d-electrons (which form band gap states slightly below the Fermi level),[22] which improves the overall surface reactivity and stability of O_V sites.[26]

Catalytic OER performances were evaluated using a thin-film rotating-disk electrode (RDE) with well-defined mass transport. It is well-known that TiO_2 is a very poor OER catalyst owing to its weak binding to oxygen intermediates,[5] which is reflected by the large onset potential (~1.9 V vs RHE) and extremely high Tafel slope 230 mV/dec (Figure 3a,b). However, the OER activity of TiO_2 is sharply improved by increasing $[Ti_{CUS}]$, characterized by the much lower onset potentials and smaller Tafel slopes. In particular, TiO_2 H-700 shows good kinetics with Tafel slope as low as 51 mV/dec, which is almost comparable to that of good OER catalysts such as Co_3O_4. Besides, TiO_2 H-700 also shows stable OER electrocatalysis with nearly 100% Faradaic efficiency (Figure S7), suggesting that the Ti_{CUS}-rich surface could work sustainably in OER catalysis. The good stability implies that the surface of TiO_2 H-700 is not easily blocked by intermediates, in line with the previous prediction from the surface reactivity characterization. Besides, alternately increasing or decreasing $[Ti_{CUS}]$ on TiO_2 results in opposite changes in OER activity (Figure 3c), emphasizing the decisive role played by Ti_{CUS} in OER catalysis. Electrochemical impedance spectroscopy (EIS) analysis dem-

DOI: 10.1021/jacs.6b05398
J. Am. Chem. Soc. 2016, 138, 9978−9985

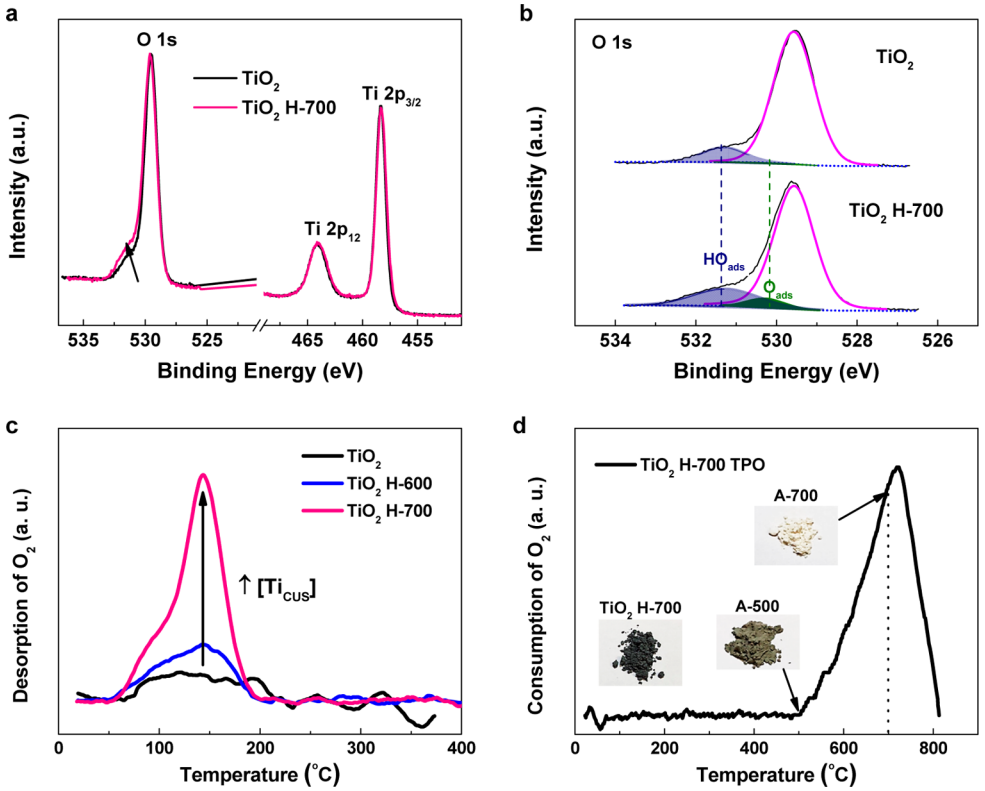

Figure 2. Surface reactivity of TiO_2 with varying density of surface Ti_{CUS}. (a) O 1s and Ti 2p XPS spectra for TiO_2 with different $[Ti_{CUS}]$. TiO_2 H-700 (with higher $[Ti_{CUS}]$) shows a more intense shoulder than that of pristine TiO_2, whereas no obvious change is observed in Ti 2p spectra. (b) Detailed O 1s spectra of pristine TiO_2 and TiO_2 H-700. A new peak, which can be assigned to dissociative adsorbed O_2 (O_{ads}), arises at about 530.2 eV (about 0.9 eV higher than lattice O) for TiO_2 H-700 together with the increase in peak intensity of dissociative adsorbed water (OH_{ads}). (c) O_2 TPD spectra for TiO_2 with varying density of surface Ti_{CUS}. (d) TPO spectrum of TiO_2 H-700. Insets show the color of original TiO_2 H-700, after calcination at 500 and 700 °C in air for 1 h, respectively. The ramping temperature of both TPD and TPO is 20 °C/min. The samples are named with treatment environment and temperature. Specifically, A and H represent the samples annealed in air and 5% H_2/Ar, respectively, and numbers are the treatment temperature.

onstrates that the OER activity is mainly determined by interfacial charge transfer resistance (R_{ct}) (Figure 3d). R_{ct} is controlled by activation energy (E_a), which is very high for pristine TiO_2 due to its weak adsorption of intermediates. The inset in Figure 3d schematically describes the mechanism of reduced E_a and thus R_{ct} by increasing $[Ti_{CUS}]$ through enhancing the adsorption of intermediates.[27] Based on these experimental results, we could confidently conclude that Ti_{CUS} could effectively alter the surface reactivity of TiO_2 and thus change its catalytic activity in OER.

2.2. Effects of $[M_{CUS}]$ on the Catalytic Performance of the TMOs with Different Surface Reactivity. The strong correlation between $[M_{CUS}]$ and surface reactivity stimulates us to examine the generality of M_{CUS} as a surface reactivity descriptor for more TMOs. We studied Co_3O_4 and α-MnO_2 as they are typical TMOs whose activities are limited by weak and strong adsorption of oxygen intermediates, respectively (Figure S1b).[6,28] Theoretically, we expect to observe the opposite influence of M_{CUS} on OER activity for the TMOs that bind oxygen intermediates too strongly or too weakly. We found that an increase in $[Co_{CUS}]$ could significantly improve the OER activity (Figure 4a,c). The Co_{CUS}-rich surface shows the best OER activity and good stability (Figure S8) ever reported for pure crystalline Co_3O_4,[29,30] whereas the Co_3O_4 oxidized in air displays poor OER activity due to reduction of $[Co_{CUS}]$ at the surface. On the contrary, for α-MnO_2, the increase of $[Mn_{CUS}]$ diminishes the OER activity, while a decrease in $[Mn_{CUS}]$ results in significantly better activity (Figure 4b,d). This trend of activity with $[M_{CUS}]$ for α-MnO_2 is totally opposite to that of Co_3O_4, but demonstrates the M_{CUS} as a surface reactivity descriptor well. Similar to TiO_2, Co_3O_4 binds to intermediates too weakly so that enhancing surface reactivity can improve its OER activity. However, the activity of α-MnO_2 can only be improved by reducing $[Mn_{CUS}]$ at the catalyst surface to weaken the strong adsorption of intermediates.

Despite the opposite trend of OER activity for Co_3O_4 and α-MnO_2 with $[M_{CUS}]$, we found that the capacitance prior to the onset of OER varies with $[M_{CUS}]$ along the same trend for both Co_3O_4 and α-MnO_2 (Figure S6c,d). Through in-depth EIS studies, we found that this variation originates from the capacitance associated with intermediates adsorption (C_{ads}) (detailed analysis can be found in the Kinetic analysis part of the Supporting Information). C_{ads} can be used to estimate the fractional surface coverage of intermediates (θ), which reflects the adsorption energy (ΔH_{ads}) of intermediates as described by eq 1.[31,32]

$$\theta \propto \exp\left(\frac{\Delta H_{ads}}{RT}\right) \quad (1)$$

Equation 1 indicates that higher ΔH_{ads} (stronger adsorption) gives rise to higher θ. Figure 4e,f shows that θ values on both Co_3O_4 and α-MnO_2 increase with increasing $[M_{CUS}]$, indicating that higher $[M_{CUS}]$ results in stronger adsorption, which agrees well with the trend of OER activity. Since experimentally

DOI: 10.1021/jacs.6b05398
J. Am. Chem. Soc. 2016, 138, 9978−9985

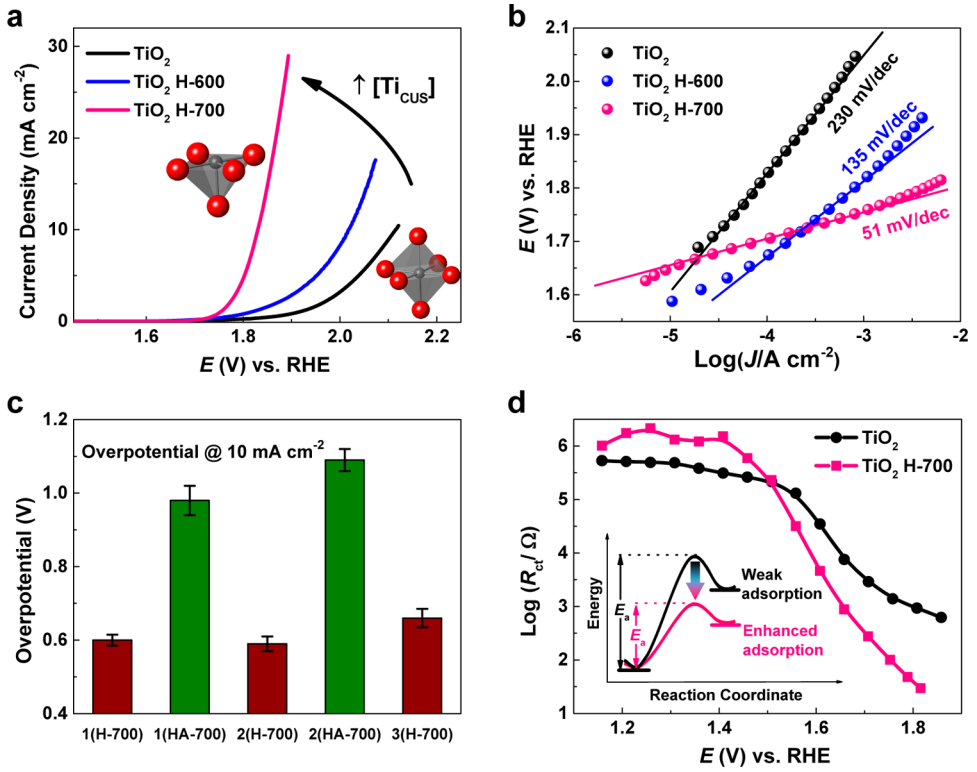

Figure 3. Electrocatalytic kinetics of TiO_2 with varying [Ti_{CUS}] in OER. (a,b) Polarization curves and Tafel plots. Inset in (a) illustrates the structure transition that is responsible for activity variation. (c) Overpotential of TiO_2 after alternate reduction and oxidation treatments to tune [Ti_{CUS}]. Here we define the reduction and subsequent oxidation (all at 700 °C) as a cycle, and the sequence of each circle is numbered by 1, 2, and 3, respectively. For example, 2(HA-700) refers to the reduced TiO_2 sample after surface oxidation in the second circle. (d) Response of charge transfer resistance (R_{ct}) to applied potential. At potential >1.6 V, R_{ct} for TiO_2 H-700 is more than 1 order of magnitude smaller than that for pristine TiO_2. The inset shows the mechanistic illustration of reduced activation energy (E_a) by enhancing intermediates adsorption. Scan rate: 5 mV s^{-1} and 1 mV s^{-1} for polarization curves and Tafel plots, respectively.

evaluating the adsorption of OER intermediates is very difficult, the θ obtained from C_{ads} could be used as an indication of adsorption energy for OER intermediates.

Moreover, the universality of M_{CUS} as a surface reactivity descriptor was further verified on α-Fe_2O_3 and NiO (Figure S9), whose activities are positively and negatively dependent on [M_{CUS}], respectively. The trends are consistent with their surface reactivities (as shown in Figure S1 b, activities of α-Fe_2O_3 and NiO are limited by low and high surface reactivity, respectively). So far, we have demonstrated M_{CUS} as an effective surface reactivity descriptor for five TMOs that are well studied in OER. The OER overpotential difference for each TMO with lowest to highest [M_{CUS}] summarized in Figure 5 indicates that M_{CUS} leads to a vast difference in OER kinetics. Such a strong dependence of surface reactivity and OER catalytic activity on [M_{CUS}] suggests that M_{CUS} could serve as an effective surface reactivity descriptor for TMOs in OER.

2.3. Electronic Origin of Surface Reactivity of TMOs. The surface structure, M_{CUS}, is practically useful in tuning the surface reactivity of TMOs. To further understand the electronic origin of this descriptor, we propose the following model based on the molecular orbital and band structure theory. Bond formation of atomic O, a key intermediate in OER, on the surface of a TMO is schematically illustrated in Figure 6. Atomic oxygen, the second highest electronegative element, behaves as an acceptor in bonding with metal cations. Adsorption sites are usually M_{CUS}[5,6,33] with the only available d valence electrons for 3d and 4d TMOs. Hence we assume that the interaction between O and TMO (restricted to 3d and 4d TMOs) is mainly contributed from the coupling of O 2p to the highest occupied d-states (denoted as E_d). As shown in Figure 6, the coupling results in bonding states and antibonding states. The bonding states are generally far below Fermi level (E_F) and fully filled, whereas the filling of antibonding states depends on the relative energy of E_d to E_F (denoted as ($E_d - E_F$)). The higher the energy of E_d relative to E_F, the less filling of the antibonding states and the stronger adsorption.

The detailed interpretation of the model is divided into three categories: n-type, p-type, and metallic TMOs. For stoichiometric n-type TMOs, E_d in the valence band is far below E_F, which results in lower energy of antibonding states relative to E_F. Thus, the antibonding states are fully filled and the adsorption is very weak. However, a surface with higher [M_{CUS}] than the stoichiometric surface can introduce band gap states (BGS) due to unpaired d-electrons (Figure 6b),[19,21,34] which can increase E_d and push the antibonding states above E_F, leading to less filling of antibonding states. Therefore, higher [M_{CUS}] gives rise to higher surface reactivity and this can be evidenced by diminished BGS upon adsorption of oxygen.[21,35] The cases of TiO_2, α-Fe_2O_3, V_2O_5,[14,36] and MoO_3[14] can be described well by Figure 6a and b. For stoichiometric p-type TMOs, E_d is close to E_F and thus antibonding states are partially filled as shown in Figure 6c. Therefore, surface reactivity of p-type TMOs is usually higher than that of stoichiometric n-type TMOs, i.e., MnO_2, Co_3O_4, and NiO can adsorb OER intermediates relatively more strongly than TiO_2 and α-Fe_2O_3 (Figure S1b). However, some p-type TMOs have

DOI: 10.1021/jacs.6b05398
J. Am. Chem. Soc. 2016, 138, 9978−9985

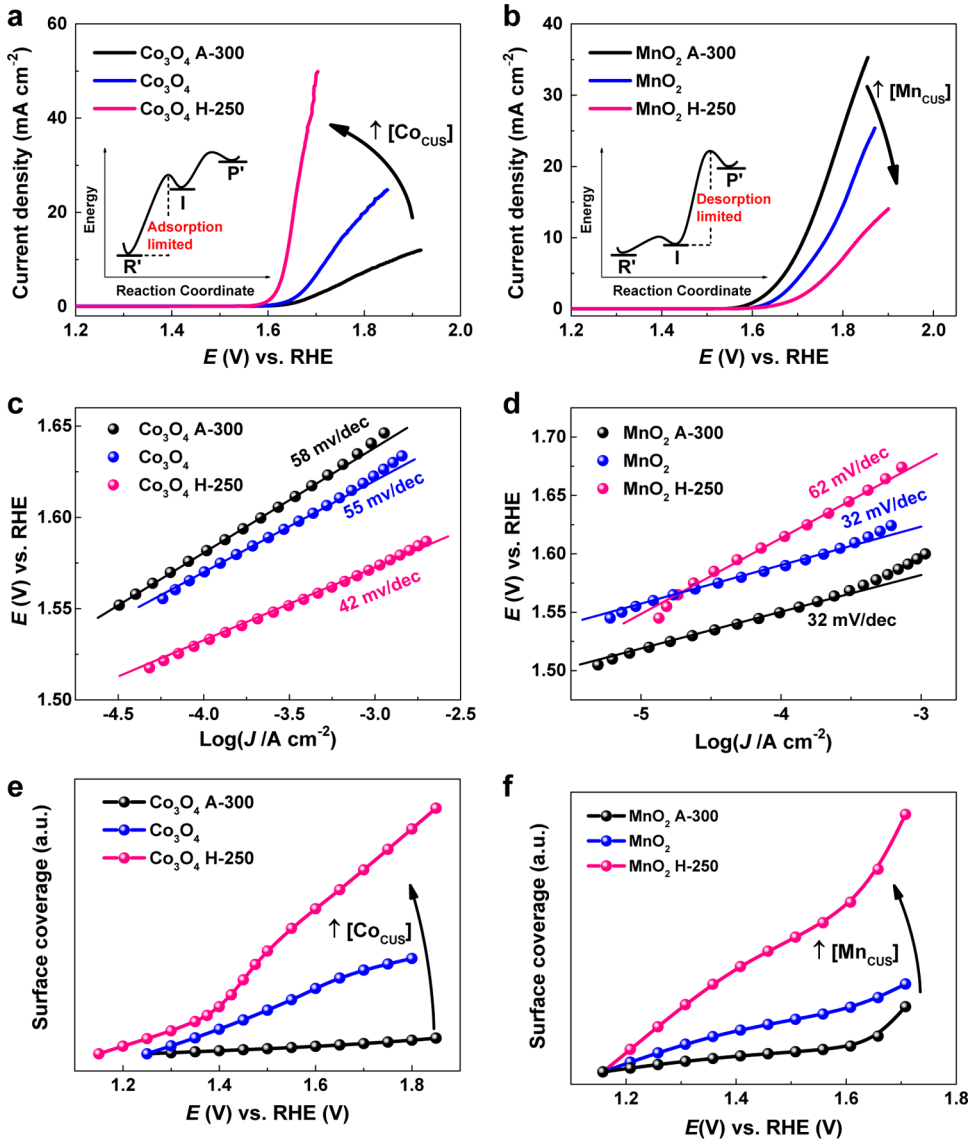

Figure 4. Electrochemical characterization of Co_3O_4 and α-MnO_2 with varying density of M_{CUS}. (a,b) OER polarization curves of Co_3O_4 (a weak-binding catalyst) and α-MnO_2 (a strong-binding catalyst). Insets show the simplified energy diagram to illustrate the rate-determining step (RDS) associated with key intermediate (I), wherein only two critical steps of adsorption and desorption of intermediate (I) are shown. Here we use R′ and P′ to represent reactant equivalent and product equivalent, respectively. The equivalent means that the transition from reactant to R′ and from P′ to product are fast. (c,d) Tafel plots for Co_3O_4 and α-MnO_2. (e,f) Variation in the surface coverage of intermediates on Co_3O_4 and α-MnO_2. Scan rate: 5 mV s^{-1} and 1 mV s^{-1} for polarization curves and Tafel plots, respectively. The naming rules of the samples are the same as that of TiO_2.

different band structures. A typical example is CuO, whose d-band in the valence band is lower than the O 2p band.[37] Therefore, coupling between Cu 3d and O 2p results in lower energy of antibonding states relative to E_F, and the antibonding states are fully filled; hence the bonding of O to CuO is the weakest among all 3d TM monoxides.[13,38] Higher [M_{CUS}] on surface of p-type TMOs also leads to higher surface reactivity in a similar way as shown in Figure 6b, which has been verified on MnO_2[39] and Co_3O_4.[29] Lower [M_{CUS}] as compared to the stoichiometric surface resulting from extra surface oxygen is also common on p-type TMOs, which leads to lower E_d relative to E_F and thus weakens the adsorption (Figure 6d). A typical case is NiO,[40] which usually presents as $Ni_{1-x}O$ due to the strong adsorption of oxygen. For metallic TMOs[14] (at room temperature) such as TiO, V_2O_3, and MoO_2, the good electrical conductivity stems from partially occupied d-states which extend to E_F.[41] As a result, this group of TMOs shows very high surface reactivity such that they will be oxidized in the presence of O_2.[6,14]

Some differences and close connections between surface reactivity of TMOs and TMs can be understood by comparing our model with the d-band theory.[9,12] One obvious difference is that the adsorption energy on TMs is contributed from the interaction of adsorbates with both s and d states of metal atoms,[9] whereas the adsorption energy on TMOs only results from the coupling of adsorbates with the highest occupied d states of metal cations. Thus, TMs show much higher surface reactivity than TMOs,[13] which explains the reason that TMs cannot work in OER catalysis. Considering the similar electronic descriptor ($E_d - E_F$) used for describing the surface reactivity for both TMs and TMOs, our model could be regarded as a generalization of the d-band theory into TMOs, which was shown to be unsuccessful in the past.[12]

DOI: 10.1021/jacs.6b05398
J. Am. Chem. Soc. 2016, 138, 9978−9985

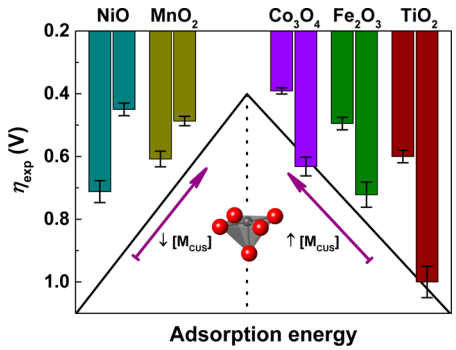

Figure 5. Overview of the overpotential dependence on surface M_{CUS} for TMOs. Only the overpotentials of TMOs with the highest and the lowest $[M_{CUS}]$ are shown for comparison. The arrows indicate the rational optimization direction: increasing $[M_{CUS}]$ for the TMOs on the right (weak binding), while reducing $[M_{CUS}]$ for the TMOs on the left (strong binding). The η_{exp} for Fe_2O_3 refers to current density = 1 mA cm^2, while that for the remaining TMOs corresponds to current density = 10 mA cm^{-2}.

3. CONCLUSION

In summary, we identified a tunable surface structure, M_{CUS}, as an effective surface reactivity descriptor for TMOs in OER. From both computational and experimental results, a viable design principle to achieve desirable OER activity on TMOs is thus deduced: for better activity, increase $[M_{CUS}]$ for the TMOs with weak intermediates adsorption, while reduce $[M_{CUS}]$ for those bind to the intermediates too strongly, and vice versa. The electronic origin of the descriptor can be interpreted by a new model proposed in this work, wherein the energy of the highest occupied d-states relative to the Fermi level serves as an (electronic structure) descriptor for surface reactivity. Our model describes the reactivity trends among various TMOs and thus can potentially initiate the development of a universal model for surface chemistry of TMOs.

4. EXPERIMENTAL SECTION

4.1. Chemicals. Semiconductor grade potassium hydroxide (KOH) (99.99% trace metal basis, Sigma-Aldrich) was used as supporting electrolyte in all electrochemical tests. The

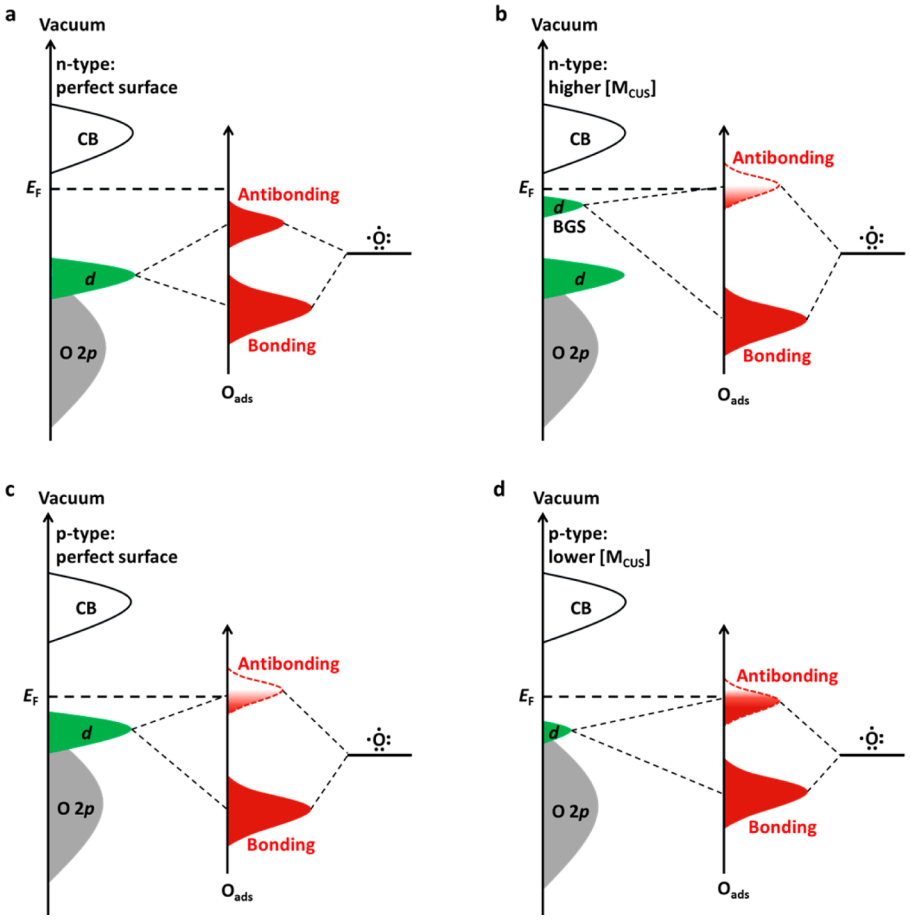

Figure 6. Schematic bond formation of atomic oxygen on different types of TMOs through coupling of O 2p to the highest occupied d-states. Most of the stable TMOs are either semiconductors or insulators, the valence band (VB) of which is composed of O 2p states and the d-states of the transition metal cation. (a,b) Bonding of O to an n-type TMO. On the stoichiometric surface of an n-type TMO, the antibonding states are usually filled due to the relatively low energy of highest occupied d-states (E_d) to the Fermi level (E_F). However, surface oxygen deficiency (higher $[M_{CUS}]$) introduce band gap states (BGS) resulted from unpaired d-electrons.[19,41] The d-states generated by higher $[M_{CUS}]$ lead to stronger adsorption of O due to upshift of the antibonding states relative to E_F. (c,d) Bonding of O to a p-type TMO. For p-type TMOs, E_d is much closer to E_F, and thus the antibonding states are less filled as compared to the stoichiometric n-type TMOs. Downshift of E_d relative to E_F results in more filling of the antibonding states, giving rise to weaker bonding. This model implies that not all d-states contribute to the bonding strength of adsorbates. Instead, only the highest occupied d-states dominate the energy of the antibonding states, and together with the Fermi level the filling of antibonding states can be defined. Thus, the $(E_d - E_F)$ should be the electronic origin of surface reactivity for TMOs.

DOI: 10.1021/jacs.6b05398
J. Am. Chem. Soc. 2016, 138, 9978−9985

electrolyte solution of 1 M KOH was prepared by dissolving the semiconductor grade KOH with 18.2 MΩ cm deionized (DI) water. The high-purity electrolyte could eliminate the influence of impurity on the intrinsic activity and properties of the catalysts studied in this work by showing no observable change during many cycles of cyclic voltammetry.

4.2. Materials Preparation. Rutile TiO_2 nanorods with exposed facets were synthesized by a modified hydrothermal method.[43] In a typical synthesis, 1 mL of titanium butoxide (97% Aldrich) was added into a mixed solution containing 30 mL of deionized (DI) water and 30 mL of hydrochloric acid (37 wt %). Twenty milligrams of P25 nanoparticles was added as seeds and dispersed in the growth solution by ultrasonication. The hydrothermal reaction was conducted in a 100 mL autoclave at 170 °C for 5 h. After the reaction, the product was washed several times with DI water and harvested by centrifugation.

The as-prepared TiO_2 nanorods were oxidized and reduced in air and hydrogen (5% H_2 mixed with Ar) to remove and create coordinatively unsaturated Ti cation sites (Ti_{CUS}) at the surface, respectively, denoted as TiO_2 A-700, H-600, and H-700, where A and H represent the air and hydrogen environment, and numbers are the treatment temperature. Structure and surface reactivity characterization of TiO_2 can be found in Figure S3 and Figure 2.

Single-crystalline Co_3O_4 nanocubes, α-Fe_2O_3 nanorhombohedrons, and α-MnO_2 nanorods were synthesized via the methods reported in the literature with slight modifications.[44−46] NiO was obtained from Sigma-Aldrich (size <50 nm, 99.8%) showing black color, indicating much excess oxygen at the surface. The density of Ni_{CUS} can be increased by calcination at high temperature to remove excess oxygen at the surface.[40] The surface reduction and oxidation conditions (e.g., temperature) were carefully chosen to only induce the atomic structure changes at the surface. As a representative of relative reducible TMOs, Co_3O_4 was treated in much lower temperature to tune the density of Co_{CUS} (structure and surface reactivity characterization are provided in Figures S4 and S5).

4.3. Materials Characterization. The crystal structure of as-prepared TMOs was analyzed by X-ray powder diffraction (Cu Kα radiation, Bruker D2 Phaser). Transmission electron microscopy (TEM) and high-resolution transmission electron microscopy (HRTEM) images were obtained on a JEOL model JEM 3010 TEM equipped with a Gatan camera. X-ray photoelectron spectroscopy (XPS) measurements were conducted on an ESCALAB 250 photoelectron spectrometer (Thermo Fisher Scientific) at 2.4×10^{-10} mbar using a monochromatic Al Kα X-ray beam (1486.60 eV). Binding energy (BE) of the element was calibrated to the BE of carbon (284.60 eV).

4.4. TPX Measurements. All measurements were carried out at a heating rate of 20 °C/min and ambient pressure on ChemBET Pulsar (ITS Science & Medical Pte Ltd.). Temperature-programmed reduction (TPR) was performed in 5% H_2/Ar (v/v) to determine the suitable temperature to create surface M_{CUS}. Temperature-programmed oxidation (TPO) was carried out in 5% O_2/He (v/v). Prior to O_2-TPD (temperature-programmed desorption) test, the samples were exposed to high-purity O_2 (99.9995%) for half an hour to let the samples reach saturated adsorption of O_2.

4.5. Electrochemical Studies. Electrochemical tests were conducted on an Autolab PGSTAT 30 with a three-electrode configuration. Saturated calomel electrode (SCE, 0.241 V vs SHE (standard hydrogen electrode)) and Pt plate (~1 cm^2) were used as the reference and counter electrode, respectively. To prepare a working electrode, the TMO samples were first dispersed in an isopropyl alcohol/water (v:v = 1:1) solution with a concentration of 2 mg/mL. The mixture was sonicated for 3 h to form a well-dispersed solution. Subsequently, 10 μL of this solution was drop-casted onto a precleaned glassy carbon (GC) rotating disk electrode (0.196 cm^2). Finally, 5 μL of 0.5 wt % Nafion solution was drop-casted onto the TMOs to fix the material. The electrodes were dried in atmosphere overnight before electrochemical tests. The electrochemical testing was conducted at a rotating speed of 1600 rpm in 1 M KOH electrolyte (pH = 13.72) to minimize mass transport limit. To reduce the effects of impurities, plastic cell and high purity KOH (semiconductor grade, 99.99% trace metals basis) were used during the electrochemical testing. In particular, for the electrochemical characterization of NiO, the KOH solution was purified to remove trace amount of Fe impurity, which has been reported to sensitively influence the electrocatalytic performance of NiO.[47] All polarization curves in this work were corrected by eliminating *iR* drop in the electrical circuit. A relatively low scan rate (5 mV s^{-1}) was employed to diminish the contribution of nonfaradic current to the current of polarization curves. The series resistance (R_s), mainly originating from ionic conduction in the electrolyte, is in the range 5.5−7.0 Ω. The potentials of polarization curves were compensated based on the following equation: $V_{RHE} = V_{SCE} + 0.241 + 0.059 \times pH - R_s \times i$.

Electrochemical impedance spectroscopy (EIS) measurements were conducted on Solartron 1287A potentiostat coupled with 1260 FRA (Frequency Response Analysis). EIS were collected in the same dc potential range as that of electrochemical tests. Ten millivolt sinusoidal wave potential perturbations were applied to the dc potential. Polarization curve was collected prior to and after sequential ac impedance tests to evaluate the reliability of the electrodes. EIS data was collected only if there was no observable change for the two curves. Polarization of working electrodes at each dc potential for 1 min was conducted to allow the system to reach steady state.

■ ASSOCIATED CONTENT

Supporting Information

The Supporting Information is available free of charge on the ACS Publications website at DOI: 10.1021/jacs.6b05398.

Computational details and kinetic analysis; Figures S1−S9 (PDF)

■ AUTHOR INFORMATION

Corresponding Authors

*slchen@whu.edu.cn.

*liubin@ntu.edu.sg.

Notes

The authors declare no competing financial interest.

■ ACKNOWLEDGMENTS

This work was supported by the fund from Nanyang Technological University startup grant: M4080977.120, Singapore Ministry of Education Academic Research Fund (AcRF) Tier 1: RG111/15, Public Sector Funding from Agency for Science, Technology and Research of Singapore (A*Star): M4070232.120, and the National Research Foundation (NRF),

DOI: 10.1021/jacs.6b05398
J. Am. Chem. Soc. 2016, 138, 9978−9985

Prime Minister's Office, Singapore under its Campus for Research Excellence and Technological Enterprise (CREATE) program. L. W. Fang and S. L. Chen are supported by the Ministry of Science and Technology of China under the National Basic Research Program (Grant No. 2012CB932800).

REFERENCES

(1) Bard, A. J.; Fox, M. A. *Acc. Chem. Res.* **1995**, *28*, 141.
(2) Weber, M. F.; Dignam, M. J. *J. Electrochem. Soc.* **1984**, *131*, 1258.
(3) Karlsson, R. K. B.; Cornell, A. *Chem. Rev.* **2016**, *116*, 2982.
(4) Koper, M. T. M. *J. Electroanal. Chem.* **2011**, *660*, 254.
(5) Rossmeisl, J.; Qu, Z. W.; Zhu, H.; Kroes, G. J.; Nørskov, J. K. *J. Electroanal. Chem.* **2007**, *607*, 83.
(6) Man, I. C.; Su, H.-Y.; Calle-Vallejo, F.; Hansen, H. A.; Martínez, J. I.; Inoglu, N. G.; Kitchin, J.; Jaramillo, T. F.; Nørskov, J. K.; Rossmeisl, J. *ChemCatChem* **2011**, *3*, 1159.
(7) Hong, W. T.; Risch, M.; Stoerzinger, K. A.; Grimaud, A.; Suntivich, J.; Shao-Horn, Y. *Energy Environ. Sci.* **2015**, *8*, 1404.
(8) Hammer, B.; Norskov, J. *Nature* **1995**, *376*, 238.
(9) Bligaard, T.; Nørskov, J. K. In *Chemical Bonding at Surfaces and Interfaces*; Nilsson, A., Pettersson, L. G. M., Nørskov, J. K., Eds.; Elsevier: Amsterdam, 2008; pp 257−278.
(10) Stamenkovic, V. R.; Mun, B. S.; Arenz, M.; Mayrhofer, K. J. J.; Lucas, C. A.; Wang, G.; Ross, P. N.; Markovic, N. M. *Nat. Mater.* **2007**, *6*, 241.
(11) Greeley, J.; Stephens, I. E. L.; Bondarenko, A. S.; Johansson, T. P.; Hansen, H. A.; Jaramillo, T. F.; Rossmeisl, J.; Chorkendorff, I.; Nørskov, J. K. *Nat. Chem.* **2009**, *1*, 552.
(12) Nørskov, J. K.; Abild-Pedersen, F.; Studt, F.; Bligaard, T. *Proc. Natl. Acad. Sci. U. S. A.* **2011**, *108*, 937.
(13) Calle-Vallejo, F.; Inoglu, N. G.; Su, H.-Y.; Martinez, J. I.; Man, I. C.; Koper, M. T. M.; Kitchin, J. R.; Rossmeisl, J. *Chem. Sci.* **2013**, *4*, 1245.
(14) Cox, P. *The surface science of metal oxides*; Cambridge University Press, 1996; pp 1−7, 158−200, and 264−266.
(15) Suntivich, J.; May, K. J.; Gasteiger, H. A.; Goodenough, J. B.; Shao-Horn, Y. *Science* **2011**, *334*, 1383.
(16) Suntivich, J.; Gasteiger, H. A.; Yabuuchi, N.; Nakanishi, H.; Goodenough, J. B.; Shao-Horn, Y. *Nat. Chem.* **2011**, *3*, 546.
(17) García-Mota, M.; Vojvodic, A.; Abild-Pedersen, F.; Nørskov, J. K. *J. Phys. Chem. C* **2013**, *117*, 460.
(18) Xu, Z.; Kitchin, J. R. *J. Chem. Phys.* **2015**, *142*, 104703.
(19) Papageorgiou, A. C.; Beglitis, N. S.; Pang, C. L.; Teobaldi, G.; Cabailh, G.; Chen, Q.; Fisher, A. J.; Hofer, W. A.; Thornton, G. *Proc. Natl. Acad. Sci. U. S. A.* **2010**, *107*, 2391.
(20) Pang, C. L.; Lindsay, R.; Thornton, G. *Chem. Rev.* **2013**, *113*, 3887.
(21) Wendt, S.; Sprunger, P. T.; Lira, E.; Madsen, G. K. H.; Li, Z.; Hansen, J. Ø.; Matthiesen, J.; Blekinge-Rasmussen, A.; Lægsgaard, E.; Hammer, B.; Besenbacher, F. *Science* **2008**, *320*, 1755.
(22) Krüger, P.; Bourgeois, S.; Domenichini, B.; Magnan, H.; Chandesris, D.; Le Fèvre, P.; Flank, A. M.; Jupille, J.; Floreano, L.; Cossaro, A.; Verdini, A.; Morgante, A. *Phys. Rev. Lett.* **2008**, *100*, 055501.
(23) Kowalski, P. M.; Camellone, M. F.; Nair, N. N.; Meyer, B.; Marx, D. *Phys. Rev. Lett.* **2010**, *105*, 146405.
(24) Epling, W. S.; Peden, C. H. F.; Henderson, M. A.; Diebold, U. *Surf. Sci.* **1998**, *412*−*413*, 333.
(25) Lira, E.; Hansen, J. Ø.; Huo, P.; Bechstein, R.; Galliker, P.; Lægsgaard, E.; Hammer, B.; Wendt, S.; Besenbacher, F. *Surf. Sci.* **2010**, *604*, 1945.
(26) Deskins, N. A.; Rousseau, R.; Dupuis, M. *J. Phys. Chem. C* **2011**, *115*, 7562.
(27) Nørskov, J. K.; Bligaard, T.; Logadottir, A.; Bahn, S.; Hansen, L. B.; Bollinger, M.; Bengaard, H.; Hammer, B.; Sljivancanin, Z.; Mavrikakis, M.; et al. *J. Catal.* **2002**, *209*, 275.
(28) Trasatti, S. *J. Electroanal. Chem. Interfacial Electrochem.* **1980**, *111*, 125.
(29) Wang, Y.; Zhou, T.; Jiang, K.; Da, P.; Peng, Z.; Tang, J.; Kong, B.; Cai, W.-B.; Yang, Z.; Zheng, G. *Adv. Energy Mater.* **2014**, *4*, 1400696.
(30) Tung, C.-W.; Hsu, Y.-Y.; Shen, Y.-P.; Zheng, Y.; Chan, T.-S.; Sheu, H.-S.; Cheng, Y.-C.; Chen, H. M. *Nat. Commun.* **2015**, *6*, 8106.
(31) Somorjai, G. A. *Introduction to surface chemistry and catalysis*; John Wiley & Sons, 1994; p 303.
(32) Ertl, G. *Reactions at Solid Surfaces*; John Wiley & Sons, Inc.: 2010; pp 1−17.
(33) García-Mota, M.; Vojvodic, A.; Metiu, H.; Man, I. C.; Su, H.-Y.; Rossmeisl, J.; Nørskov, J. K. *ChemCatChem* **2011**, *3*, 1607.
(34) Sánchez-Sánchez, C.; Garnier, M. G.; Aebi, P.; Blanco-Rey, M.; de Andres, P. L.; Martín-Gago, J. A.; López, M. F. *Surf. Sci.* **2013**, *608*, 92.
(35) Zhang, W.; Liu, L.; Wan, L.; Liu, L.; Cao, L.; Xu, F.; Zhao, J.; Wu, Z. *Phys. Chem. Chem. Phys.* **2015**, *17*, 20144.
(36) Zhang, Z.; Henrich, V. E. *Surf. Sci.* **1994**, *321*, 133.
(37) Ghijsen, J.; Tjeng, L. H.; van Elp, J.; Eskes, H.; Westerink, J.; Sawatzky, G. A.; Czyzyk, M. T. *Phys. Rev. B: Condens. Matter Mater. Phys.* **1988**, *38*, 11322.
(38) Xu, Z.; Kitchin, J. R. *Catal. Commun.* **2014**, *52*, 60.
(39) Cheng, F.; Zhang, T.; Zhang, Y.; Du, J.; Han, X.; Chen, J. *Angew. Chem., Int. Ed.* **2013**, *52*, 2474.
(40) Kotsev, N. K.; Ilieva, L. I. *Catal. Lett.* **1993**, *18*, 173.
(41) Greiner, M. T.; Helander, M. G.; Tang, W.-M.; Wang, Z.-B.; Qiu, J.; Lu, Z.-H. *Nat. Mater.* **2011**, *11*, 76.
(42) Chrétien, S.; Metiu, H. *J. Phys. Chem. C* **2011**, *115*, 4696.
(43) Liu, B.; Aydil, E. S. *J. Am. Chem. Soc.* **2009**, *131*, 3985.
(44) Chen, H. M.; Liu, R.-S.; Li, H.; Zeng, H. C. *Angew. Chem., Int. Ed.* **2006**, *45*, 2713.
(45) Liu, X.; Zhang, J.; Wu, S.; Yang, D.; Liu, P.; Zhang, H.; Wang, S.; Yao, X.; Zhu, G.; Zhao, H. *RSC Adv.* **2012**, *2*, 6178.
(46) Su, D.; Ahn, H.-J.; Wang, G. *J. Mater. Chem. A* **2013**, *1*, 4845.
(47) Trotochaud, L.; Young, S. L.; Ranney, J. K.; Boettcher, S. W. *J. Am. Chem. Soc.* **2014**, *136*, 6744.

DOI: 10.1021/jacs.6b05398
J. Am. Chem. Soc. 2016, 138, 9978−9985